

Article

# Uptake Fluoride from Water by Starch Stabilized Layered Double Hydroxides

Jiming Liu, Xiuping Yue \*, Xinyu Lu and Yu Guo

College of Environment Science and Engineering, Taiyuan University of Technology, Taiyuan 030024, China; liujiming@tyut.edu.cn (J.L.); luxinyu@tyut.edu.cn (X.L.); tyut2002489@126.com (Y.G.)

\* Correspondence: yuexiuping@tyut.edu.cn; Tel.: +86-351-6010-243

Received: 14 May 2018; Accepted: 4 June 2018; Published: 7 June 2018



**Abstract:** A novel starch stabilized Mg/Al layered Double hydroxides (S-LDHs) was prepared in a facile approach and its fluoride ion removal performance was developed. Characterization of S-LDHs was employed by using X-ray diffraction (XRD), Fourier-transform infrared spectroscopy (FTIR), and particle size distribution. The adsorption property was studied through the assessment of the adsorption isotherms, kinetic models, thermal dynamics, and pH influence. The result shows that a low loading of starch of 10 mg onto layered double hydroxides (LDHs) could obviously improve the fluoride removal rate. The S-LDHs had three times higher the adsorption capacity to fluoride than that of Mg/Al LDHs to fluoride. The particle size was smaller and the particle size distribution was narrower for S-LDHs than that for Mg/Al LDHs. The Langmuir adsorption isotherm model and pseudo-second-order kinetic model fitted well with the experimental data. In thermodynamic parameters, the enthalpy ( $\Delta H^0$ ) value was  $35.63\text{ kJ}\cdot\text{mol}^{-1}$  and the entropy ( $\Delta S^0$ ) value was  $0.0806\text{ kJ}\cdot\text{mol}^{-1}\text{K}^{-1}$ . The values of  $\Delta G^0$  were negative, implying the adsorption process is spontaneous. S-LDHs reveals stable adsorption property in a wide pH range from 3 to 9. The mechanism for fluoride adsorption on S-LDHs included surface adsorption and interaction ion exchange.

**Keywords:** layered double hydroxides; hydrotalcite; starch; fluoride; adsorption property; thermodynamics

## 1. Introduction

Many reports indicate high fluoride content exists in drinking water in many countries such as China, Russia, Pakistan, and South Africa [1–3]. Use of drinking water containing high concentrations of fluoride can cause dental fluorosis, nervous system diseases, and even cancer [4–6]. The world health organization (WHO) has set the guideline on fluoride in drinking water at  $1.5\text{ mg/L}$  [7]. Plenty of methods have been attempted to lower high levels of fluoride, including electrodialysis [8], adsorption [9–12], precipitation [13], ion exchange [14] and membrane filtration [15]. Among them, adsorption is found to be a more appropriate method to remove the fluoride in drinking water due to the fact that it is relatively simple in design and convenient to operate.

In recent years, Layered double hydroxides (LDHs) have attracted increasing attention in catalysis, adsorption, ion exchange, etc., and have been regarded as an effective adsorbent in reducing the contents of excessive anions, including fluoride [12,16–18]. LDHs are composed of alternating stacked cationic layers and interlayer compensation anions. The basic structural formula is:  $M^{2+}_{1-x}M^{3+}_x(OH)_2(A^{n-})_{x/n}\cdot mH_2O$ , wherein  $M^{2+}$  and  $M^{3+}$  represent divalent and trivalent cations, respectively, and  $A^{n-}$  represents an n-valent anion. Typical LDHs are  $Mg_6Al_2(OH)_{16}CO_3^{2-}\cdot 4H_2O$ , which have a structure similar to brucite  $Mg(OH)_2$ , and consist of  $Mg^{2+}$  and  $Al^{3+}$  ions on both sides, with  $CO_3^{2-}$  anion and water molecules in the middle, like sandwich bread. LDHs own a large interlayer

surface, which can capture all kinds of different exchangeable anionic species, provide it with a high removal efficiency of anionic compounds. However, investigation shows that carbonate anion ( $\text{CO}_3^{2-}$ ) is easily generated by  $\text{CO}_2$  in the air, enters the intermediate layer and its strong affinity prevents the substitution of other anions unless it is further calcined, thus leading to LDHs that cannot be regarded as exchangeable inorganic anionic materials [19]. It has been reported that the removal rate of fluoride ions by Mg/Al LDHs is only 29.8% [20].

To overcome these drawbacks, a kind of corn starch was applied to the preparation of synthesizing starch-stabilized LDHs, and its usage in fluoride removal was examined. The starch-stabilized nanoparticles have many merits and have received worldwide attention because of their good biodegradability, environmental friendliness, and low cost [21]. The starch-based materials exhibited much less agglomeration and greater reactivity than those without starch, thereby accelerating the physical property of the compounds. Liang and Zhao studied the removal of  $\text{AsO}_4^{2-}$  by a starch stabilized magnetite and the results showed that the adsorption capacity of the stabilized magnetite is 14% higher than that of original magnetite [22]. Therefore, in this present work, a novel starch stabilized Mg/Al LDHs material (S-LDHs) was developed to study its fluoride ion removal performance. Characterization of S-LDHs was employed by using X-ray diffraction (XRD), Fourier-transform infrared spectroscopy (FTIR), and particle size distribution. The adsorption mechanism was studied through the assessment of adsorption isotherms, kinetic models, thermal dynamics, and pH influence.

## 2. Materials and Methods

### 2.1. Reagents and Synthesis of Adsorbents

The reagents utilized in this study were of analytical grade (A.R.). The aqueous solutions were employed with deionized water. The Mg/Al layer double hydroxides were synthesized using the co-precipitation method [23]. Starch stabilized layered double hydroxides (S-LDHs) were synthesized by the modified co-precipitation method. Firstly, 10 mg of starch was dispersed in 1000 mL aqueous solution to form a starch solution. Secondly, a combined solution of 0.50 mol of  $\text{Al}(\text{NO}_3)_3 \cdot 9\text{H}_2\text{O}$  and 1.50 mol of  $\text{Mg}(\text{NO}_3)_2 \cdot 6\text{H}_2\text{O}$  and a combined solution of 0.5 mol/L  $\text{Na}_2\text{CO}_3$  and 2.00 mol/L NaOH was mixed with starch solution slowly accompanied with vigorous stirring to maintain the pH at around 10. Subsequently, the suspension was aged, separated, and dried. Lastly, the resulting material passed through a 60 mesh screen and was collected for later use.

### 2.2. Characterization Methods

The material's surface features were obtained by FTIR spectrums on a Bruker TENSOR27 spectrophotometer (Bruker International AG, Rheinstetten, Baden-Württemberg, Germany) within the limit of 400–4000  $\text{cm}^{-1}$ . The materials elements were analyzed by XRD patterns in a Bruker D8 X (Bruker International AG, Rheinstetten, Baden-Württemberg, Germany). The scanning scope is 5–80° every 0.02° ( $2\theta$ ) with a step speed of 8°·min<sup>-1</sup>. The particle size distribution was determined by Zetasizer NANO ZS90 (Enigma Business Park, Worcestershire, United Kingdom) with the maximum particle size range of 0.3 nm–10  $\mu\text{m}$ , a concentration range of 0.1 ppm–40% *w/v*, and a detection angle of 175°, 12.8°.

### 2.3. Experimental Procedure

Adsorption experiments were investigated in a lab-scale application. Adsorption isotherms were gained by mixing 0.2 g S-LDHs with 50 mL of water with fluoride a concentration of 10 mg/L, 20 mg/L, 50 mg/L, 80 mg/L, and 100 mg/L and the fluoride concentrations under equilibrium conditions were tested after 4 h of reaction. The kinetics experiment of fluoride adsorption was obtained with the dosage of S-LDHs 0.2 g combined with an initial fluoride concentration of 10 mg/L in a conical flask with 50 mL of water. The residual fluoride concentration was measured after a different contact time.

The experiments were done in a thermostat with continuous oscillation at 180 rpm,  $20 \pm 1^\circ\text{C}$ . After the reaction the adsorbent was separated by filtration.

The adsorption value of fluoride on S-LDHs could be calculated as follows [24]:

$$q_e = \frac{(C_0 - C_e)V}{W} \quad (1)$$

where  $q_e$  is the amount of fluoride adsorbed on the S-LDHs at equilibrium time;  $C_0$  (mg/L) is the initial fluoride concentration, and  $C_e$  (mg/L) is the equilibrium fluoride concentration;  $V$  is the volume of solution (L); and  $W$  is the weight of adsorbent (g).

### 3. Results and Discussion

#### 3.1. Characteristics of LDHs

Representative XRD patterns of the Mg-Al LDHs and starch-based LDHs adsorbents are displayed in Figure 1. It can be seen that Mg-Al LDHs materials displays sharp peaks in (003), (006), and (013), showing that the materials are the characteristic reflections of the double layer hydroxide structures (Figure 1a). As for the samples with starch stabilized, the characteristics of the original diffraction peak still exist, but the peak value is weakened and the width of the characteristic peak is broadened, indicating that the material has changed (Figure 1b). The XRD patterns after the fluoride adsorption are shown in Figure 1c. The peaks in (003), (006), and (009) become wider and the peak strength becomes weaker, which shows that the material crystallinity reduced after the adsorption.

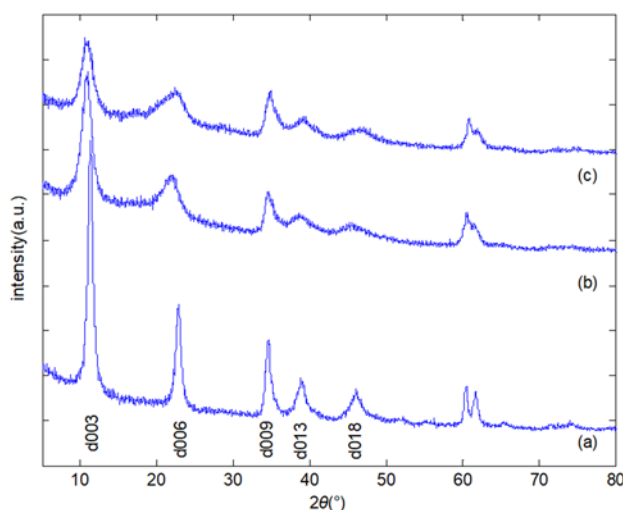


**Figure 1.** X-ray Diffraction (XRD) pattern of (a) Mg/Al LDHs, (b) S-LDHs, (c) Samples after fluoride removal on S-LDHs.

The FTIR study of Mg-Al LDHs, S-LDHs and S-LDHs before and after adsorption were exhibited to detect the presence of characteristic functional groups. As can be seen from Figure 2a in the FTIR spectrum, the region between  $3400$  and  $3700\text{ cm}^{-1}$  has broad bands for the -OH stretching vibrations of the hydroxyl groups [25]. The band at  $1653\text{ cm}^{-1}$  is for the adsorbed inter-layer water. The peak at  $1372\text{ cm}^{-1}$  is for the vibration of  $\text{CO}_3^{2-}$  and  $\text{NO}_3^-$ . The band below  $1000\text{ cm}^{-1}$  is for the metal bands. While for the FTIR spectrum of S-LDHs (Figure 2b), the weak band at  $\sim 1315\text{ cm}^{-1}$  and  $\sim 1030\text{ cm}^{-1}$  is assigned to  $\text{CH}_2-\text{O}-\text{CH}_2$  [26], indicating that starch and LDHs effectively bonded together. The FTIR spectra of the S-LDHs after fluoride adsorption are shown in Figure 2c. The band at  $3503\text{ cm}^{-1}$  shifted to  $3468\text{ cm}^{-1}$ , showing that the anions and the hydroxyl groups interacted on the adsorbent.

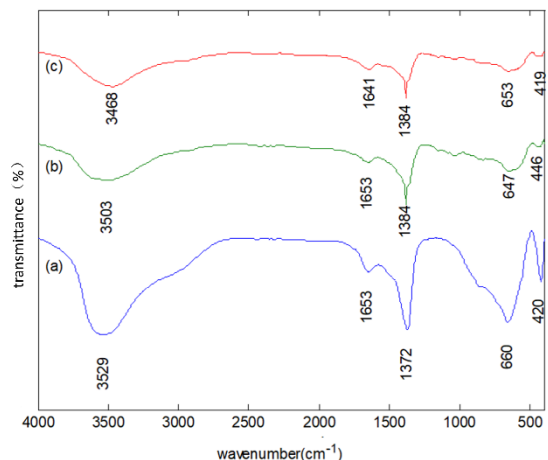


**Figure 2.** Fourier-transform infrared spectroscopy (FTIR) pattern of (a) Mg/Al LDHs, (b) S-LDHs, (c) Samples after fluoride removal on S-LDHs.

The particle size distribution of Mg/Al LDHs and S-LDHs is shown in Figure 3. It can be seen that the average diameter is 1358 nm and the particle size distribution is scattered. The average particle size of S-LDHs was 421 nm, and the particle size distribution was relatively concentrated, which showed that the particle size distribution of the stabilized starch was more uniform.

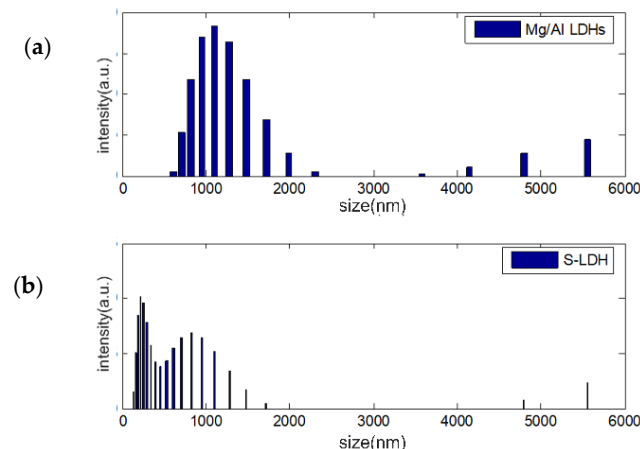


**Figure 3.** Size distribution of Mg/Al LDHs (a) and S-LDHs (b).

### 3.2. Adsorption Study

#### 3.2.1. Dosage Effect of Starch Content

The dosage effect of the starch on the fluoride removal is displayed in Figure 4. It can be seen that the starch content has an obvious effect on the fluoride removal. The removal rate increased greatly with the increment of the starch dosage. When the dosage amount of the starch is about 10 mg, the removal percentage of the fluoride reached 98%, which is three times higher than the removal rate of the Mg/Al LDHs. The first reason is that the starch is in an anion state under alkaline condition, inhibiting the entry of carbon dioxide and increasing the removal rate of the fluoride. The second reason is that the starch promotes the higher dispersion of LDHs, thus increasing the surface area of S-LDHs and making the adsorption point more abundant.

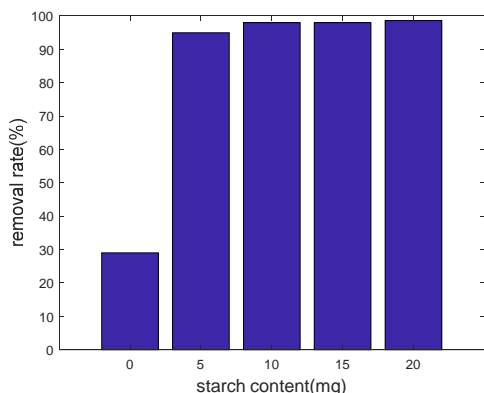


**Figure 4.** Effect of starch content on fluoride removal.

### 3.2.2. Adsorption Isotherm

The experimental adsorption data of the fluoride on S-LDHs is determined by the isotherm models of Langmuir and Freundlich [27]. The Langmuir isotherm model supports monolayer adsorption, and the Freundlich isotherm is related to the multi-layer, non-linear adsorption process. The correlation coefficient ( $R^2$ ) and the root mean square error (RMSE) are compared and evaluated, which is the best fit of the two isotherms.

The linearized expression of the Langmuir isotherm is:

$$\frac{C_e}{q_e} = \frac{C_e}{q_m} + \frac{1}{K_L q_m} \quad (2)$$

The linearized expression of the Freundlich isotherm is:

$$\ln q_e = \ln K_F + \frac{1}{n} \ln C_e \quad (3)$$

where  $q_m$  is the calculated adsorption amount (mg/g);  $K_L$  is the Langmuir constant (L/mg).  $K_F$  is the Freundlich constant;  $1/n$  is the heterogeneity factor.

RMSE was calculated for evaluating the straight line fit and the equation is as follows [28]:

$$\text{RMSE} = [\sum (q_t - q_t^*)^2 / (n - m)]^{0.5} \quad (4)$$

where  $q_t$  is the adsorbed (mg/g) at time  $t$  gained from the lab experiments, and  $q_t^*$  is the fluoride capacity adsorbed (mg/g) forecasted by the two models. The samples number is expressed by the  $n$  value and fitted parameters number is expressed by the  $m$  value.

Figure 5 and Table 1 show the results of the isotherm curves fitting with the Freundlich and Langmuir equations. The results showed that the Langmuir isotherm model had a higher  $R^2$  and lower RMSE value, which indicated that the reaction process might be a monolayer adsorption with chemisorption on the adsorbent surface. It can be seen that the maximum adsorption capacity is 21.72 mg/g, which is three times higher than the value of previously investigated for Mg/Al LDHs. The value of  $K_L$  was greater than zero, indicating that the adsorption system was favorable.

**Table 1.** Isotherm adsorption models of fluoride onto S-LDHs.

| Langmuir Isotherm |              |        |        | Freundlich Isotherm |        |        |        |
|-------------------|--------------|--------|--------|---------------------|--------|--------|--------|
| $K_L$             | $q_m$ (mg/g) | $R^2$  | RMSE   | $K_F$               | $n$    | $R^2$  | RMSE   |
| 0.123             | 21.72        | 0.9987 | 0.0102 | 2.719               | 1.7393 | 0.9884 | 0.0804 |

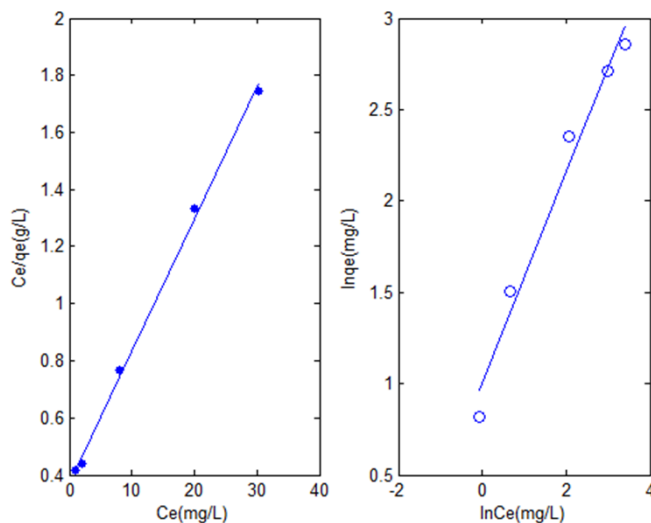


**Figure 5.** Curve fit of Langmuir and Freundlich isotherm.

### 3.2.3. Adsorption Kinetic Studies

The adsorption kinetics can identify the process of the adsorption efficiency and help to verify the fluoride adsorption mechanism. The adsorption rate and fluoride uptake kinetics on S-LDHs were studied based on two reaction based models (pseudo first and pseudo second) and a diffusion based model (intraparticle diffusion model). The pseudo-first order model assumes the reaction is reversible, the pseudo-second order model regards chemisorption as the rate limiting step. The intraparticle diffusion assumes that the plots pass through origin. The models can be expressed as follows [29]:  
pseudo-first order model [30]

$$\ln (q_e - q_t) = \ln (q_e) - k_1 t \quad (5)$$

pseudo-second order model [31]

$$\frac{t}{q_t} = \frac{1}{k_2 q_e^2} + \frac{t}{q_e} \quad (6)$$

intraparticle diffusion model [32]

$$q_t = K_F t^{1/2} + C \quad (7)$$

The common parameters,  $k_1$  represents the rate constant of adsorption ( $\text{min}^{-1}$ ) obtained from the plot of  $\ln(q_e - q_t)$  against  $t$ .  $k_2$  means the pseudo-second rate constant ( $\text{g}/(\text{mg}\cdot\text{min})$ ) obtained from the linear plot of  $t/q_t$  against  $t$ .  $K_F$  is the intraparticle diffusion rate constant ( $\text{mg}/(\text{g}\cdot\text{min}^{0.5})$ ).

The results of the fitting kinetics models were summarized in Figure 6 and Table 2. A pseudo-second order kinetic was proved to be fitted with the experiment data by the high  $R^2$  ( $>0.99$ ) and low RMSE, which implied chemisorption. The values of  $k_2$  were low, indicating that the adsorption process rates were fast.

**Table 2.** Adsorption kinetic models for fluoride removal on S-LDHs and the calculated constants.

| Kinetic Models          |   | Parameter           |        |        |
|-------------------------|---|---------------------|--------|--------|
| Pseudo-first-order      | $k_1 (\text{min}^{-1})$                           | $q_e (\text{mg/g})$ | $R^2$  | RMSE   |
|                         | 0.0771  | 2.036               | 0.9872 | 0.2401 |
| Pseudo-second-order     | $k_2 (\text{g}/(\text{mg}\cdot\text{min}))$       | $q_e (\text{mg/g})$ | $R^2$  | RMSE   |
|                         | 0.1467  | 2.6107              | 0.9995 | 0.1194 |
| intraparticle diffusion | $k_F (\text{mg}/(\text{g}\cdot\text{min}^{0.5}))$ | $R^2$               | RMSE   | -      |
|                         | 2.4289  | 0.8471              | 0.7321 | -      |

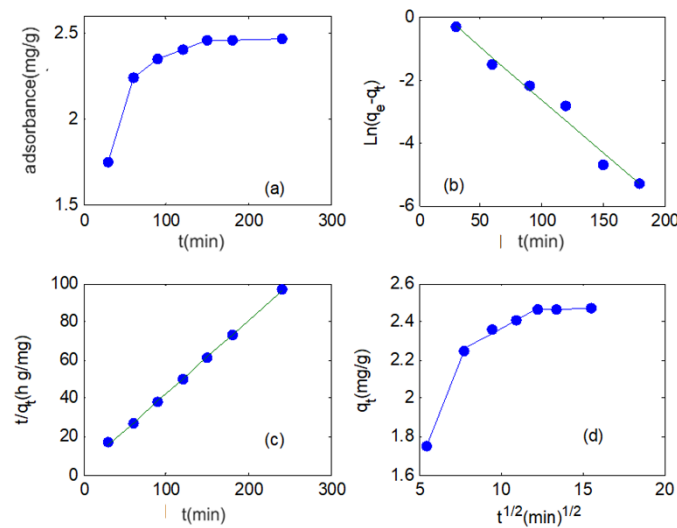


**Figure 6.** Kinetics of fluoride adsorption on the S–LDHs from (a) experiment, models by (b) pseudo first, (c) pseudo second, and (d) intraparticle diffusion.

### 3.2.4. Adsorption Thermodynamic Studies

The variation of temperature can be used to analyze the thermodynamic properties of LDHs–fluoride interaction. In this study, temperature was controlled in a range of 20–50 °C.  $\Delta G^0$ ,  $\Delta S^0$  and  $\Delta H^0$  were calculated by the Van't Hoff equation:

$$\Delta G^0 = -RT\ln b, \quad (8)$$

$$\Delta G^0 = \Delta H^0 - T\Delta S^0, \quad (9)$$

$$\ln b = \frac{\Delta S^0}{R} - \frac{\Delta H^0}{RT}, \quad (10)$$

where,  $R$  is the universal gas constant ( $8.314 \text{ J}\cdot\text{mol}^{-1} \text{ K}^{-1}$ ),  $b$  is adsorption isothermy constant,  $\Delta G^0$  is the change in free energy,  $\Delta H^0$  is the standard enthalpy and  $\Delta S^0$  is the standard entropy,  $T$  is the temperature (K). Here,  $b$  value can be calculated from the Langmuir constant  $K_L \cdot Q_m$ .  $\Delta H^0$  and  $\Delta S^0$  parameters can be obtained, respectively, from the slope and intercept of the plot of  $\ln b$  vs.  $1/T$ . The results are shown in Table 3. It can be seen that the values of  $\Delta G^0$  are negative, indicating the sorption process is spontaneous in nature. As the temperature rises, the reaction becomes relatively easy. The positive value of  $\Delta H^0$  confirms the sorption process is endothermic. The positive value of  $\Delta S^0$  indicates that the reaction is spontaneous, and the solid-liquid interface is random at the time of adsorption.

**Table 3.** The value of thermodynamic parameter for the adsorption of fluoride by the S-LDHs.

| Temperature (°C) | $b$  | Thermodynamic Parameter |                       |                          |
|------------------|------|-------------------------|-----------------------|--------------------------|
|                  |      | $\Delta G^0$ (kJ/mol)   | $\Delta H^0$ (kJ/mol) | $\Delta S^0$ (J/(mol·K)) |
| 20               | 9.73 | -12.44                  |                       |                          |
| 30               | 4.25 | -10.78                  |                       |                          |
| 40               | 2.67 | -9.93                   | 35.63                 | 0.0806                   |
| 50               | 2.55 | -10.12                  |                       |                          |

Arrhenius equation representing the variance between the temperature and the activation energy of adsorption. The activation energy calculation can be obtained using the Formula (11).

$$k = Ae^{-E_a/RT}, \quad (11)$$

where,  $k$  is the pseudo second-order reaction rate constant, ( $\text{g}/(\text{mg}\cdot\text{min})$ ),  $E_a$  is activation energy, ( $\text{kJ/mol}$ ). The calculated activation energy is 38.83  $\text{kJ/mol}$ , greater than 20  $\text{kJ/mol}$ , indicating the reaction is corresponded to the slow defluorination stage, controlled by the chemical reaction of the fluoride ion and S-LDHs.

### 3.3. Mechanism Analysis

pH value is an important parameter for reflecting the adsorption property. In this paper, the isoelectric point ( $\text{pH}_{\text{PZC}}$ ) and variance of the pH value was used to analyze the proposed adsorption mechanism.  $\text{pH}_{\text{PZC}}$  plays an important role on the surface properties of the material, determining the degree of difficulty of adsorption. The  $\text{pH}_{\text{PZC}}$  of adsorbent can be determined by the salt supplement method [33]. As shown in Figure 7, the  $\text{pH}_{\text{PZC}}$  of the S-LDHs adsorbents is 9.22. The results of the variance of the initial pH value to the fluoride adsorption on S-LDH at 20 °C were also analyzed. It can be seen that with the initial pH value in the solution varying from 3.0 to 9.0, the adsorption capacity of the fluoride onto the material remained stable, while when the pH value was higher than 9.0, the adsorption capacity of the fluoride decreased gradually, but still kept a comparably high level, indicating that a wide range of initial pH value has little effect on the removal ability of fluoride. When the pH value is less than the  $\text{pH}_{\text{PZC}}$ , the charge surface is positively charged, while when pH value is higher than  $\text{pH}_{\text{PZC}}$ , the charge surface is negatively charged. Thus the possible reason is as follows: under acidic conditions, the protonation makes the surface of the adsorbent positively charged, and fluoride ions are more easily adsorbed onto S-LDHs. Under alkaline conditions, the  $\text{OH}^-$  concentration in the solution increases, and competes with the fluoride ion, indicating that the fluoride ions could not effectively enter the layer of the S-LDHs. The reason why the removal rate of the fluoride ions is still high under alkaline conditions is that the surface of the starch is positively charged and the fluoride ions are efficiently adsorbed. In summary, according to the adsorption experiments and the characterization analysis, fluoride ion adsorption by S-LDHs is presumed mainly by the interaction of the LDHs and the surface adsorption of S-LDHs.

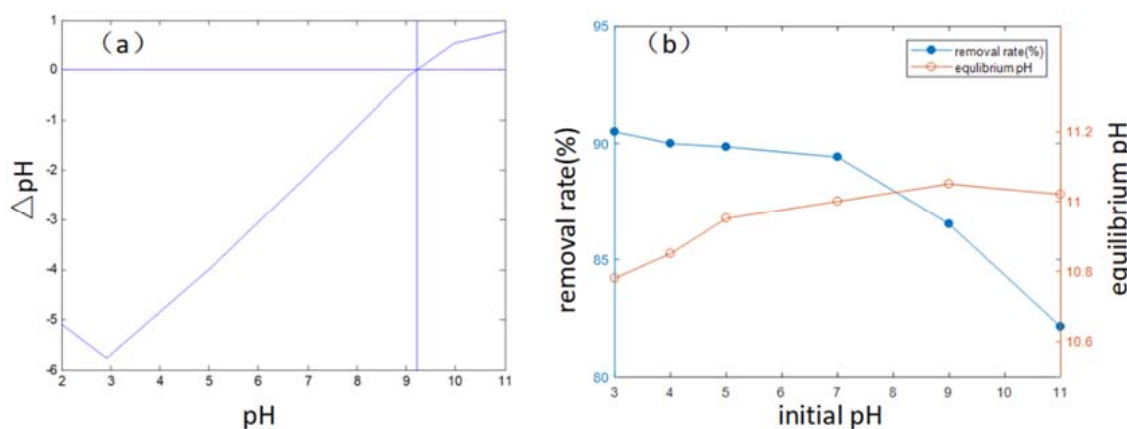


**Figure 7.**  $\text{pH}_{\text{PZC}}$  of S-LDHs (a) and the effect of initial pH (b) on fluoride removal.

## 4. Conclusions

In this work, starch stabilized Mg-Al-LDHs were utilized as adsorbents and the properties of Mg/Al LDHs and S-LDHs were compared. The fluoride adsorption capacity of the S-LDHs was three times higher than that of the Mg/Al LDHs. The particle size distribution of the S-LDHs is more

uniform than that of the LDHs. The Langmuir adsorption isotherm model and pseudo-second-order kinetic model fit well with the experimental data. In the thermodynamic parameters, the enthalpy ( $\Delta H^0$ ) value was 35.63 kJ mol<sup>-1</sup> and the entropy ( $\Delta S^0$ ) value was 0.0806 kJ mol<sup>-1</sup>K<sup>-1</sup>. The negative values of  $\Delta G^0$  indicated the spontaneous nature of adsorption. The change in a wide range of initial pH values has little effect on the removal ability of the fluoride. The mechanism for fluoride removal on the S-LDHs included surface adsorption and interaction ion exchange. Further investigations could focus on the reuse of the material and a dynamic monitor using real water.

**Author Contributions:** Conceptualization, J.L. and X.Y.; Methodology, J.L.; Validation, J.L., and X.Y.; Formal Analysis, Y.G.; Investigation, Y.G.; Data Curation, X.L.; Writing-Original Draft Preparation, J.L.; Writing-Review & Editing, X.L.; Supervision, X.Y.; Project Administration, X.Y.; Funding Acquisition, J.L.

**Funding:** This research was funded by Shanxi Provincial Natural Science Foundation, China, grant number 201601D102037.

**Acknowledgments:** The authors are grateful for the financial support from Shanxi Provincial Natural Science Foundation, China (Grant No. 201601D102037).

**Conflicts of Interest:** There are no conflict to declare.

## References

- Chen, P.; Wang, T.; Xiao, Y.; Tian, E.; Wang, W.; Zhao, Y.; Tian, L.; Jiang, H.; Luo, X. Efficient fluoride removal from aqueous solution by synthetic Fe-Mg-La tri-metal nanocomposite and the analysis of its adsorption mechanism. *J. Alloy. Compd.* **2018**, *738*, 118–129. [[CrossRef](#)]
- Theiss, F.L.; Couperthwaite, S.J.; Ayoko, G.A.; Frost, R.L. A review of the removal of anions and oxyanions of the halogen elements from aqueous solution by layered double hydroxides. *J. Colloid Interface Sci.* **2014**, *417*, 356–368. [[CrossRef](#)] [[PubMed](#)]
- Sakhare, N.; Lunge, S.; Rayalu, S.; Bakardjiva, S.; Subrt, J.; Devotta, S.; Labhsetwar, N. Defluoridation of water using calcium aluminate material. *Chem. Eng. J.* **2012**, *203*, 406–414. [[CrossRef](#)]
- Zhu, X.; Yang, C.; Yan, X. Metal-organic framework-801 for efficient removal of fluoride from water. *Microporous Mesoporous Mater.* **2018**, *259*, 163–170. [[CrossRef](#)]
- Gao, C.; Yu, X.; Luo, T.; Jia, Y.; Sun, B.; Liu, J.; Huang, X. Millimeter-sized Mg-Al-LDH nanoflake impregnated magnetic alginate beads (LDH-n-MABs): A novel bio-based sorbent for the removal of fluoride in water. *J. Mater. Chem. A* **2014**, *2*, 2119–2128. [[CrossRef](#)]
- He, J.; Chen, J.P. A zirconium-based nanoparticle: Essential factors for sustainable application in treatment of fluoride containing water. *J. Colloid Interface Sci.* **2014**, *416*, 227–234. [[CrossRef](#)] [[PubMed](#)]
- WHO World Health Organization. *Guidelines for Drinking-Water Quality*, 4th ed.; World Health Organization: Geneva, Switzerland, 2011; p. 371.
- Grzegorzek, M.; Majewska-Nowak, K. The influence of organic matter on fluoride removal efficiency during the electrodialysis process. *Desalination Water Treat.* **2017**, *69*, 153–162.
- Yu, Z.; Xu, C.; Yuan, K.; Gan, X.; Feng, C.; Wang, X.; Zhu, L.; Zhang, G.; Xu, D. Characterization and adsorption mechanism of ZrO<sub>2</sub> mesoporous fibers for health-hazardous fluoride removal. *J. Hazard. Mater.* **2018**, *346*, 82–92. [[PubMed](#)]
- Jiang, H.; Zhang, W.; Chen, P.; He, Q.; Li, M.; Tian, L.; Tu, Z.; Xu, Y. One Pot Method to Synthesize a Novel La-Zr Composite with Exceptionally High Fluoride Removal Performance. *J. Inorg. Organomet. Polym.* **2016**, *26*, 285–293.
- Kang, D.; Yu, X.; Ge, M. Morphology-dependent properties and adsorption performance of CeO<sub>2</sub> for fluoride removal. *Chem. Eng. J.* **2017**, *330*, 36–43. [[CrossRef](#)]
- Wan, D.; Liu, Y.; Xiao, S.; Chen, J.; Zhang, J. Uptake fluoride from water by calcined Mg-Al-CO<sub>3</sub> hydrotalcite: Mg/Al ratio effect on its structure, electrical affinity and adsorptive property. *Colloids Surfaces A* **2015**, *469*, 307–314. [[CrossRef](#)]

13. Liu, S.; Ye, X.; He, K.; Chen, Y.; Hu, Y. Simultaneous removal of Ni(II) and fluoride from a real flue gas desulfurization wastewater by electrocoagulation using Fe/C/Al electrode. *J. Water Reuse Desalin.* **2017**, *7*, 288–297. [[CrossRef](#)]
14. Markovski, J.; Garcia, J.; Hristovski, K.D.; Westerhoff, P. Nano-enabling of strong-base ion-exchange media via a room-temperature aluminum (hydr)oxide synthesis method to simultaneously remove nitrate and fluoride. *Sci. Total Environ.* **2017**, *599–600*, 1848–1855. [[CrossRef](#)] [[PubMed](#)]
15. Agbaje, T.A.; Al-Gharabli, S.; Mavukkandy, M.O.; Kujawa, J.; Arafat, H.A. PVDF/magnetite blend membranes for enhanced flux and salt rejection in membrane distillation. *Desalination* **2018**, *436*, 69–80. [[CrossRef](#)]
16. Teixeira, M.A.; Mageste, A.B.; Dias, A.; Virtuoso, L.S.; Siqueira, K.P.F. Layered double hydroxides for remediation of industrial wastewater containing manganese and fluoride. *J. Clean Prod.* **2018**, *171*, 275–284. [[CrossRef](#)]
17. Chubar, N.; Gilmour, R.; Gerda, V.; Mičušík, M.; Omastova, M.; Heister, K.; Man, P.; Fraissard, J.; Zaitsev, V. Layered double hydroxides as the next generation inorganic anion exchangers: Synthetic methods versus applicability. *Adv. Colloid Interface* **2017**, *245*, 62–80. [[CrossRef](#)] [[PubMed](#)]
18. Hu, P.; Zhang, Y.; Lv, F.; Tong, W.; Xin, H.; Meng, Z.; Wang, X.; Chu, P.K. Preparation of layered double hydroxides using boron mud and red mud industrial wastes and adsorption mechanism to phosphate. *Water Environ. J.* **2017**, *31*, 145–157. [[CrossRef](#)]
19. Shan, R.; Yan, L.; Yang, K.; Hao, Y.; Du, B. Adsorption of Cd(II) by Mg-Al-CO<sub>3</sub>- and magnetic Fe<sub>3</sub>O<sub>4</sub>/Mg-Al-CO<sub>3</sub>-layered double hydroxides: Kinetic, isothermal, thermodynamic and mechanistic studies. *J. Hazard. Mater.* **2015**, *299*, 42–49. [[CrossRef](#)] [[PubMed](#)]
20. Moriyama, S.; Sasaki, K.; Hirajima, T. Effect of calcination temperature on Mg-Al bimetallic oxides as sorbents for the removal of F- in aqueous solutions. *Chemosphere* **2014**, *95*, 597–603. [[CrossRef](#)] [[PubMed](#)]
21. Xu, L.; Chen, G.; Peng, C.; Qiao, H.; Ke, F.; Hou, R.; Li, D.; Cai, H.; Wan, X. Adsorptive removal of fluoride from drinking water using porous starch loaded with common metal ions. *Carbohydr. Polym.* **2017**, *160*, 82–89. [[CrossRef](#)] [[PubMed](#)]
22. Liang, Q.; Zhao, D. Immobilization of arsenate in a sandy loam soil using starch-stabilized magnetite nanoparticles. *J. Hazard. Mater.* **2014**, *271*, 16–23. [[CrossRef](#)] [[PubMed](#)]
23. Lv, L. Defluoridation of drinking water by calcined MgAl-CO<sub>3</sub> layered double hydroxides. *Desalination* **2007**, *208*, 125–133. [[CrossRef](#)]
24. Swain, S.K.; Patnaik, T.; Singh, V.K.; Jha, U.; Patel, R.K.; Dey, R.K. Kinetics, equilibrium and thermodynamic aspects of removal of fluoride from drinking water using meso-structured zirconium phosphate. *Chem. Eng. J.* **2011**, *171*, 1218–1226. [[CrossRef](#)]
25. Sun, Z.; Park, J.; Kim, D.; Shin, C.; Zhang, W.; Wang, R.; Rao, P. Synthesis and Adsorption Properties of Ca-Al Layered Double Hydroxides for the Removal of Aqueous Fluoride. *Water Air Soil Pollut.* **2017**, *228*, 23.
26. Mandal, S.; Mayadevi, S. Cellulose supported layered double hydroxides for the adsorption of fluoride from aqueous solution. *Chemosphere* **2008**, *72*, 995–998. [[CrossRef](#)] [[PubMed](#)]
27. Zhao, W.; Chen, Y.; Zhang, W. Rapid and convenient removal of fluoride by magnetic magnesium-aluminum-lanthanum composite: Synthesis, performance and mechanism. *Asia Pac. J. Chem. Eng.* **2017**, *12*, 640–650. [[CrossRef](#)]
28. Halajnia, A.; Oustan, S.; Najafi, N.; Khataee, A.R.; Lakzian, A. Adsorption-desorption characteristics of nitrate, phosphate and sulfate on Mg-Al layered double hydroxide. *Appl. Clay Sci.* **2013**, *80–81*, 305–312. [[CrossRef](#)]
29. Vazquez Mejia, G.; Solache-Rios, M.; Martinez-Miranda, V. Removal of fluoride and arsenate ions from aqueous solutions and natural water by modified natural materials. *Desalination Water Treat.* **2017**, *85*, 271–281.
30. El-Said, G.F.; El-Sadaawy, M.M.; Aly-Eldeen, M.A. Adsorption isotherms and kinetic studies for the defluoridation from aqueous solution using eco-friendly raw marine green algae, *Ulva lactuca*. *Environ. Monit. Assess.* **2018**, *190*, 1–15. [[CrossRef](#)] [[PubMed](#)]

31. Türker, O.C.; Baran, T. A combination method based on chitosan adsorption and duckweed (*Lemna gibba* L.) phytoremediation for boron (B) removal from drinking water. *Int. J. Phytoremediat.* **2018**, *20*, 175–183.
32. Ren, G.; Wang, X.; Huang, P.; Zhong, B.; Zhang, Z.; Yang, L.; Yang, X. Chromium (VI) adsorption from wastewater using porous magnetite nanoparticles prepared from titanium residue by a novel solid-phase reduction method. *Sci. Total Environ.* **2017**, *607*, 900–910. [CrossRef] [PubMed]
33. Dayananda, D.; Sarva, V.R.; Prasad, S.V.; Arunachalam, J.; Ghosh, N.N. Preparation of CaO loaded mesoporous Al<sub>2</sub>O<sub>3</sub>: Efficient adsorbent for fluoride removal from water. *Chem. Eng. J.* **2014**, *248*, 430–439. [CrossRef]



© 2018 by the authors. Licensee MDPI, Basel, Switzerland. This article is an open access article distributed under the terms and conditions of the Creative Commons Attribution (CC BY) license (<http://creativecommons.org/licenses/by/4.0/>).